Anomalous ζ Potential in Foam Films

Laurent Joly,* François Detcheverry, and Anne-Laure Biance
Institut Lumière Matière, UMR5306 Université Lyon 1-CNRS, Université de Lyon, 69622 Villeurbanne, France
(Received 20 June 2014; published 20 August 2014)

Electrokinetic effects offer a method of choice to control flows in micro- and nanofluidic systems. While a rather clear picture of these phenomena exists now for the liquid-solid interfaces, the case of liquid-air interfaces remains largely unexplored. Here, we investigate at the molecular level electrokinetic transport in a liquid film covered with ionic surfactants. We find that the ζ potential, quantifying the amplitude of electrokinetic effects, depends on the surfactant coverage in an unexpected way. First, it increases upon lowering surfactant coverage from saturation. Second, it does not vanish in the limit of low coverage but instead approaches a finite value. This behavior is rationalized by taking into account the key role of interfacial hydrodynamics, together with an ion-binding mechanism. We point out implications of these results for the strongly debated measurements of the ζ potential at free interfaces and for electrokinetic transport in liquid foams.

DOI: 10.1103/PhysRevLett.113.088301 PACS numbers: 82.70.Rr, 47.57.jd, 47.61.-k, 83.50.Lh

Electrokinetic (EK) phenomena take place in the vicinity of interfaces, where the presence of ionized groups results in a locally charged layer in the liquid. This electric double layer (EDL) can be set in motion by an electric field, eventually inducing through viscosity a flow known as electro-osmosis. Such EK effects, which also include streaming current and potential, are not only relevant in the biological realm [1], where charged or polar lipid bilayers are ubiquitous, but have also gained in the last decade major technological importance. Electric driving of liquids in micro- and nanochannels has indeed become the method of choice in many fluidic applications such as colloid or macromolecule separation, or miniaturized energy conversion devices [2–4].

As a coupling effect between electrostatics and hydrodynamics, EK effects, which are quantified by the ζ potential [5], depend not only on the electrostatic potential at the interface but also on the boundary condition that applies there for the flow, possibly involving some slip [6]. Implications have been examined theoretically [7,8], as well as characterized experimentally [9,10], for the liquid-solid interface. In contrast, the effect of the hydrodynamic boundary condition in the case of liquid-gas interfaces remains largely unexplored. Yet, they depart in two important ways from their solid counterpart. First, whereas at a solid wall, a no-slip boundary condition usually applies, friction with the gas is very low, thus allowing for large slip. Second, charges are not fixed to a wall but carried by species such as surfactants, which are mobile. Both differences point to the importance of a complete characterization of EK phenomena in those systems, widely encountered in industrial processes such as water purification through electrically driven bubbles [11], mineral flotation, and foam fractionation. These new effects could also be exploited to control bubble flow in liquid-filled microchannels and to design new self-assembled materials such as foams stable against drainage [12], which is nowadays a subject of active study [13,14]. More fundamentally, as the sign and magnitude of the surface potential at an air (or oil)-water interface remains strongly debated [15,16], a careful analysis of the relationship between ζ potential measurements often carried on [17,18], and exact charge borne by these fluid interfaces must be performed.

In order to get a better insight into these questions, this work investigates EK effects in foam films, where the surface charge is carried by ionic surfactants. While the distribution of such mobile surfactants will itself depend on the flow [19] and may vary according to the specific experimental setup considered, here, we focus on the basic feature that is common to all situations: the relative motion between the surfactants and the liquid. Using molecular dynamics simulations of films of aqueous electrolytes coated with a typical surfactant, we characterize the ζ potential and find a dependence on surfactant coverage very different from that expected at a liquid-solid interface. We show that this behavior can be rationalized on the basis of simple arguments that account for the specificity of the liquid-air interface.

We considered water + salt (NaCl) films coated with sodium dodecyl sulfate (SDS) surfactants; see Fig. 1(a). Periodic boundary conditions were used in the film plane, with box dimensions $L_x = L_y = 4.6$ nm. Water molecules, Na^+ ions, and DS^- surfactants were modeled following Bresme and Faraudo [20,21]. In particular, the extended simple point charge (SPC/E) model of water was used, for its good dielectric and hydrodynamic representativity, at reasonably low computational cost. An additional ingredient with regard to Refs. [20,21] concerns Cl^- ions, which were modeled consistently with Na^+ ions, using the parameters of Dang [22]. Two salt concentrations have

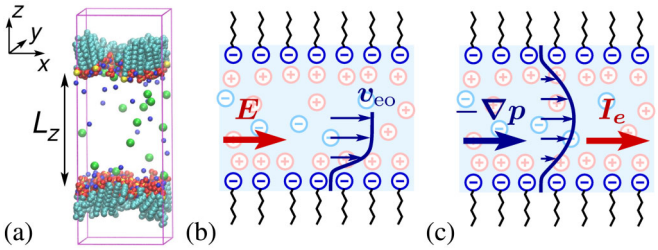

FIG. 1 (color online). (a) Snapshot of a typical system ($\lambda_D = 0.57$ nm, $c = 3.0$ nm^{-2}); water molecules are not represented. (b),(c) Sketches of electro-osmosis (EO) and streaming current (SC) numerical experiments in foam films.

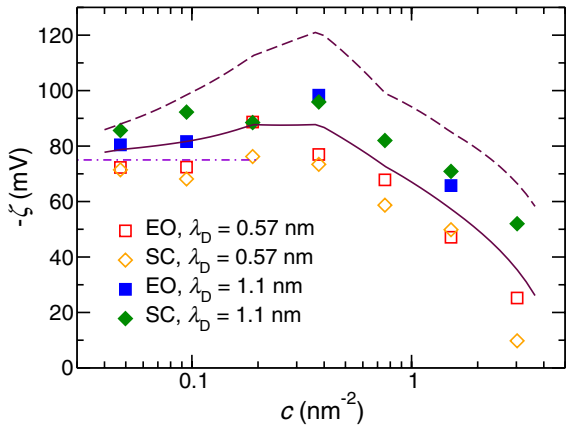

FIG. 2 (color online). ζ potential as a function of surfactant coverage c, measured from EO and SC simulations, for two Debye lengths λ_D. The solid and dashed lines are predictions from Eq. (2), for $\lambda_D = 0.57$ and 1.1 nm, respectively. The dot-dashed line is the dilute limit given by Eq. (3).

been considered $\rho_s = 0.26M$ and $0.068M$ with corresponding Debye lengths (the width of the EDL) $\lambda_D = 0.57$ and 1.1 nm. The height of the films, along the z direction, was fixed to $L_z = 10\lambda_D$, in order to ensure no EDL overlap. For each salt concentration, the surface density of surfactants c was varied from 0.047 to 3.0 nm^{-2}, with a corresponding surface charge Σ ranging from -7.6 to -480 mC/m^2. As a comparison, surface densities up to 2.2 nm^{-2} have been measured experimentally in the absence of salt [23]. The simulations were performed using LAMMPS [24]. Simulation details can be found in the Supplemental Material [25].

Two types of numerical experiments have been performed on these systems [see Figs. 1(b) and 1(c)]: streaming current (SC) and electro-osmosis (EO). In the former configuration, a Poiseuille flow is induced in the x direction, and the resulting electric current is measured. To induce the flow, a gravitylike force, adding up to F, was applied to the liquid atoms, and a counterforce adding up to $-F$ was applied to the surfactant atoms. The ionic current I_e was then measured in the surfactants' reference frame and the ζ potential computed from the standard formula: $I_e/\mathcal{A} = (\varepsilon\zeta/\eta)(-\nabla p)$. Here, $\mathcal{A} = L_y L_z$ is the film cross section, ε and η are the permittivity and dynamic viscosity of the liquid, and $-\nabla p = F/(L_x L_y L_z)$ is the force applied to the liquid per unit volume. The viscosity was computed in the same simulations from the curvature of the Poiseuille velocity profile. As regards the dielectric constant, we used the tabulated value for bulk SPC/E water at 300 K: $\varepsilon_r = 70$ [26,27]. EO numerical experiments were also performed, applying an electric field in the x direction and measuring the resulting EO flow. The applied electric field E_x ranged from 0.05 to 0.2 V nm^{-1}, depending on the surfactant coverage, to ensure that the system response remained linear with the forcing. We considered the relative motion between the liquid and the surfactant layers to compute the EO velocity v_{EO} in the middle of the film and obtained the ζ potential from $v_{\mathrm{EO}}/E_x = \varepsilon\zeta/\eta$. For each situation, we ran three independent simulations from distinct initial configurations, in order to reduce statistical uncertainties.

Figure 2 presents the evolution of the ζ potential as a function of the surfactant coverage, obtained for two Debye lengths and from both EO and SC measurements. Within uncertainties, data from the two approaches match quantitatively, as required by Onsager's reciprocal relations [28,29]. The results shown in Fig. 2 display a number of striking features. First, at high surfactant coverage, the ζ potential is much smaller than what could have been expected from the large surface charge at stake. Then, when the surfactant concentration decreases, the ζ potential *increases*. Finally, the ζ potential reaches a constant value in the limit of vanishing coverage.

To understand those results, we start by focusing on the hydrodynamic boundary condition at the interface and quantify the relative motion between the liquid and the surfactant layer. The latter is revealed more clearly in the SC case, i.e., when a Poiseuille flow is induced in the system. In Fig. 3(a), we plot the liquid velocity profiles in the reference frame of the surfactant layers for various surfactant coverages. In the central part of the film, one can observe a characteristic parabolic profile. However, the liquid velocity does not vanish at the level of the surfactant layers, as it would at most solid surfaces, where a no-slip boundary condition applies. Instead, the velocity profile displays a plateau that extends across the surfactant-laden interface. Keeping in mind that we plotted the velocity profiles in the reference frame of the surfactants, this plateau value corresponds to a velocity jump between the liquid and the surfactant layer. This velocity jump, or slip velocity, will be denoted by v_s in the following. One can also define the shear plane, where the extrapolated parabolic profile reaches v_s, and whose position will be denoted by z_s. Finally, the observed velocity jump is usually discussed in terms of the so-called partial slip boundary condition [6], which relates the slip velocity v_s to

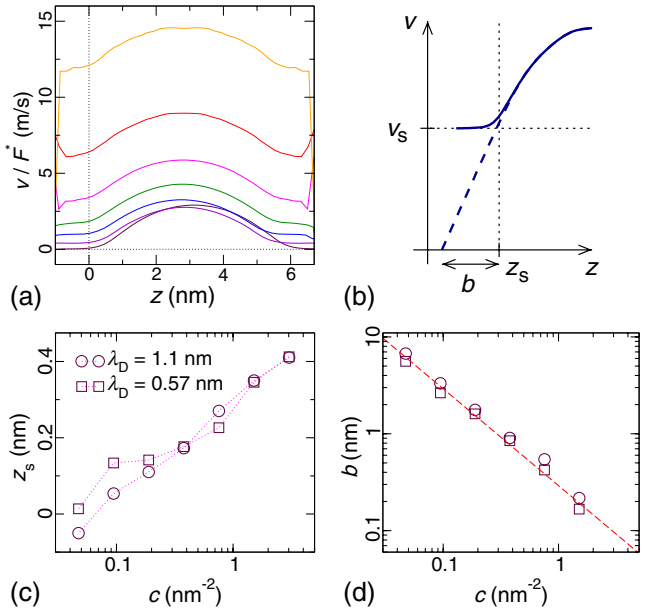

FIG. 3 (color online). Top: (a) Poiseuille velocity profiles in the SC configuration ($\lambda_D = 0.57$ nm), for increasing surfactant coverage c from top to bottom. The velocity is measured in the surfactant reference frame and divided by the normalized applied force $F^* = F/F(c = 0.047\ \mathrm{nm}^{-2})$ for comparison purposes. The origin of the z axis is taken at the average position of the surfactant sulfur atoms. (b) Cartoon illustrating the characterization of the hydrodynamic boundary condition. Bottom: (c) Shear plane position z_s and (d) slip length b as a function of the surfactant coverage, for two Debye lengths λ_D. The slip length is fitted using Eq. (1) (dashed line).

the shear rate $\dot{\gamma}(z) = \partial_z v$ at the shear plane [see Fig. 3(b)]: $v_s = b\dot{\gamma}(z_s)$, with b the slip length.

Figures 3(c) and 3(d) sum up our measurements of the shear plane position z_s and slip length b, for both Debye lengths considered and all surfactant densities. As observed and discussed earlier by some of us [8,30], the hydrodynamic boundary condition does not depend significantly on the Debye length. On the other hand, it is strongly affected by the surfactant coverage. As shown in Fig. 3(d), the slip length decreases as $b \propto c^{-1}$, a behavior that can be rationalized with a simple picture [31]. If the fluid moves with velocity v_s with respect to the surfactant heads, the total friction force per unit area is $\mathcal{F} = \alpha\eta R v_s c$, where R is a characteristic size and α a dimensionless, geometric factor. Since, by definition, $\mathcal{F} = \eta/b \times v_s$ [6], one gets $b = 1/(\alpha R c)$. While this argument *a priori* holds only in the dilute limit, when the contributions from each surfactant can be added, it describes the simulation data almost up to the highest surface coverage considered, i.e., close to saturation. For definiteness, the surfactant heads are now idealized as half-sphere, for which $\alpha = 3\pi$, giving

$$b = \frac{1}{3\pi R c}, \tag{1}$$

where the hydrodynamics radius obtained by fitting the numerical results is $R = 0.364$ nm, the correct order of magnitude expected from the head dimensions. As regards the shear plane position [Fig. 3(c)], a monotonic shift toward the film interior is observed upon increasing the surfactant density. This trend can be qualitatively understood as detailed in the Supplemental Material [25] and plays a significant role in the ζ potential, as shown below.

We now turn to the ion distribution in the EDL. Figure 4 displays typical charge and water density profiles for low and high surfactant coverage and shows that the surfactant-laden interface differs from a standard solid surface in several ways. In contrast to the liquid-solid case, where charges are fixed to a wall of given geometry, here, the surfactant heads carrying the charge can fluctuate in position with respect to the liquid-air interface and the entire interface can deform due to capillary waves [32]. Both effects contribute to the widening of the charge distribution [33] observed in Fig. 4. Another striking feature is the nearly complete overlap between the ionic and surfactant charge distributions at high coverage. Analysis of numerical molecular configurations (see the Supplemental Material [25]) shows that in that case, most ions are bound to the surfactant heads. The fraction θ of such bound ions, shown in the inset, vanishes at low coverage but approaches unity close to saturation. This ion binding can be described phenomenologically, as detailed in the Supplemental Material [25].

Focusing now on the ζ potential, we extend previous approaches [8,35,36] to the case of surfactant-laden interfaces. We consider the SC situation for simplicity, but the results are directly transferable to EO, according to Onsager's reciprocal relations [28,29]. The streaming current I_e in the foam film is twice the current originating

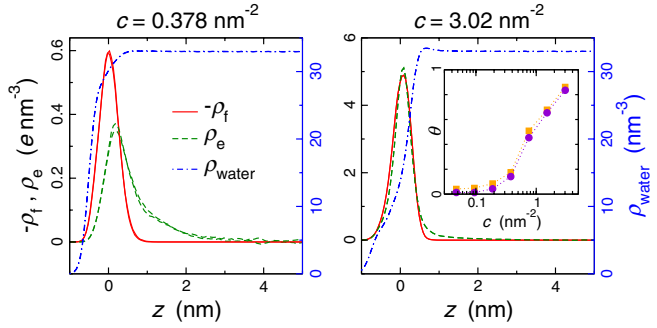

FIG. 4 (color online). Typical charge density profiles of surfactants and ions, for $\lambda_D = 1.1$ nm and two surfactant coverages c. The solid red lines represent the absolute surfactant charge $|\rho_f| = -\rho_f$. The dashed green lines represent the ionic charge ρ_e. The dash-dotted blue lines represent the water density profile. Each data set is plotted for both the SC and EO simulations. The origin of the z axis is taken at the average position of the surfactant sulfur atoms. Inset: Fraction of bound ions θ versus surfactant coverage c, for $\lambda_D = 1.1$ and 0.57 nm (violet circles and orange squares, respectively).

at one surface, which can be written as the integral over the interface of the electric current density: $I_e = 2L_y \int \rho_e(z) v(z) dz$, where L_y is the width of the interface, $\rho_e(z)$ the ionic charge density, and $v(z)$ the liquid velocity. The velocity profile is approximated as $v(z) = v_s + \dot{\gamma}(z - z_s)H(z - z_s)$, where H is the Heaviside function, $v_s = \dot{\gamma} b$, and $\dot{\gamma}$ is the shear rate at z_s. This profile is the superposition of a plug flow at constant velocity v_s and a "no-slip" part that neglects the curvature of the velocity profile at the scale of the EDL. Accordingly, the ζ potential can be decomposed into slip and no-slip contributions $\zeta = \zeta_{\text{slip}} + \zeta_{\text{no-slip}}$. The slip contribution corresponds to the plug flow of the whole ionic charge $\int \rho_e dz = -\Sigma$ at velocity v_s and writes $\zeta_{\text{slip}} = \Sigma b/\varepsilon$, independently of the ionic charge distribution. To evaluate the no-slip contribution, as a first approximation, we neglect the spatial distribution of the surfactant and take $\rho_f(z) = \Sigma\delta(z)$. Following traditional approaches [4,5] yields $\zeta_{\text{no-slip}} = V(z_s)$, where V is the electrostatic potential. The total ζ potential then reads

$$\zeta = \zeta_{\text{slip}} + \zeta_{\text{no-slip}} = \frac{\Sigma b}{\varepsilon} + V(z_s). \tag{2}$$

In the limit of low surfactant coverage, the no-slip contribution $\zeta_{\text{no-slip}}$ becomes negligible. Indeed, as we checked from numerical results by charge density integration, it approaches the Debye-Hückel result $\Sigma\lambda_D/\varepsilon$, as soon as $\Sigma \lesssim 30$ mC/m^2. The no-slip contribution being proportional to the surface charge, it vanishes in the dilute limit. On the other hand, combining Eqs. (1) and (2), and taking $\Sigma = -ec$, since ion binding is negligible at low coverage, one gets

$$\zeta(c \to 0) = -\frac{e}{3\pi R\epsilon}. \tag{3}$$

Interestingly, the surface charge and slip length dependence on the surfactant coverage in the slip contribution compensate exactly in the dilute limit, and the ζ potential reaches a finite value for vanishing surfactant coverage. Even though saturation of slip length can result in nonmonotonic variation of the ζ potential [30,37,38], a finite value in the limit of vanishing surface charge is unknown for the liquid-solid interface. Furthermore, a numerical estimate of Eq. (3) yields a value of -75 mV, in good agreement with numerical results; see Fig. 2. Importantly, this suggests that even very few impurities on a bare interface can generate a non-negligible ζ potential, whose magnitude depends on impurity size and charge. This effect might play an important role in the understanding of EK measurements of surface charge near free interfaces [16].

Finally, we use Eq. (2) to estimate the ζ potential over the whole range of surfactant coverage. In doing so, we assume that bound ions completely cancel the surfactant charge, leading to an apparent charge $\Sigma = -ec(1 - \theta)$. For the potential $V(z)$, we take the exact solution to the Poisson-Boltzmann equation for a single wall. Taking Eq. (1) for the slip length and the simulation results for z_s and θ yields the theoretical curves shown in Fig. 2. While they consistently overestimate the simulation results, they capture the main trend as a function of coverage and Debye length, with a collapse at high c induced by ion binding. In view of the crudeness of the model (see the Supplemental Material for an improved but somewhat *ad hoc* description [25]), the agreement is reasonable. This suggests that to recover the unusual dependence of the ζ potential, the three main ingredients are the slip length dependence $b \propto c^{-1}$, the shift in shear plane position z_s, and the ion binding.

As a conclusion, we have characterized at the molecular level electrokinetic effects at a foam film interface and its dependence on surfactant coverage. We find a nontrivial and nonconventional dependence, the ζ potential tending to decrease upon increasing the surface charge. Strikingly, in the dilute limit, the slippage contribution compensates exactly for the decrease in surface charge, resulting in a saturation value of the ζ potential around 75 mV in our case. This value is significant, as experimental values for the ζ potential typically fall in the range 0–150 mV. Because they point out the key role of impurities even at very low density, our findings are relevant for the understanding of surface potential measurements on free interfaces [16,39], most notably, water [17,18], which remain highly debated [15]. Overall, this study is a first step toward a complete understanding of electrokinetics near surfactant-laden interfaces. Having characterized locally the relative motion between liquid and surfactants, one can now address the situation where the global surfactant distribution is inhomogeneous and induces Marangoni flow. Electrokinetics with surfactants as mobile charge carriers may induce a variety of effects, all at play in a liquid foam.

We thank Lydéric Bocquet and Christophe Ybert for fruitful discussions throughout the completion of this work. This study was supported by the French Agence Nationale de la Recherche (ANR) through the E-FOAM Project. We are grateful for the computing resources of JADE (CINES, French National HPC), obtained through Project No. c20132a7167, and of the PSMN (Pôle Scientifique de Modélisation Numérique) Computing Center of ENS de Lyon.

*laurent.joly@univ-lyon1.fr

[1] H. Daiguji, Chem. Soc. Rev. **39**, 901 (2010).
[2] T. M. Squires and S. R. Quake, Rev. Mod. Phys. **77**, 977 (2005).
[3] R. B. Schoch, J. Y. Han, and P. Renaud, Rev. Mod. Phys. **80**, 839 (2008).
[4] L. Bocquet and E. Charlaix, Chem. Soc. Rev. **39**, 1073 (2010).

[5] R. J. Hunter, *Foundations of Colloid Science*, 2nd ed. (Oxford University, Oxford, England, 2001).
[6] L. Bocquet and J. L. Barrat, Soft Matter **3**, 685 (2007).
[7] V. M. Muller, I. P. Sergeeva, V. D. Sobolev, and N. V. Churaev, Colloid J. USSR **48**, 606 (1986).
[8] L. Joly, C. Ybert, E. Trizac, and L. Bocquet, Phys. Rev. Lett. **93**, 257805 (2004).
[9] C. I. Bouzigues, P. Tabeling, and L. Bocquet, Phys. Rev. Lett. **101**, 114503 (2008).
[10] M. C. Audry, A. Piednoir, P. Joseph, and E. Charlaix, Faraday Discuss. **146**, 113 (2010).
[11] S. E. Burns, S. Yiacoumi, and C. Tsouris, Separation and Purification Technology **11**, 221 (1997).
[12] O. Bonhomme, O. Liot, A.-L. Biance, and L. Bocquet, Phys. Rev. Lett. **110**, 054502 (2013).
[13] V. Miralles, B. Selva, I. Cantat, and M.-C. Jullien, Phys. Rev. Lett. **112**, 238302 (2014).
[14] E. Chevallier, A. Saint-Jalmes, I. Cantat, F. Lequeux, and C. Monteux, Soft Matter **9**, 7054 (2013).
[15] R. Vacha, V. Buch, A. Milet, P. Devlin, and P. Jungwirth, Phys. Chem. Chem. Phys. **9**, 4736 (2007).
[16] K. Roger and B. Cabane, Angew. Chem., Int. Ed. Engl. **51**, 5625 (2012).
[17] P. Creux, J. Lachaise, A. Graciaa, J. K. Beattie, and A. M. Djerdjev, J. Phys. Chem. B **113**, 14 146 (2009).
[18] M. Takahashi, J. Phys. Chem. B **109**, 21 858 (2005).
[19] D. Langevin, Annu. Rev. Fluid Mech. **46**, 47 (2014).
[20] F. Bresme and J. Faraudo, Langmuir **20**, 5127 (2004).
[21] F. Bresme and J. Faraudo, Mol. Simul. **32**, 1103 (2006).
[22] L. X. Dang, J. Am. Chem. Soc. **117**, 6954 (1995).
[23] V. Bergeron, Langmuir **13**, 3474 (1997).
[24] S. Plimpton, J. Comput. Phys. **117**, 1 (1995); http://lammps.sandia.gov/.
[25] See Supplemental Material at http://link.aps.org/supplemental/10.1103/PhysRevLett.113.088301 for simulation details, an improved model for the zeta potential, a detailed discussion of the ion binding phenomenon and a simple model for the shift of the shear plane.
[26] M. R. Reddy and M. Berkowitz, Chem. Phys. Lett. **155**, 173 (1989).
[27] D. J. Bonthuis and R. R. Netz, J. Phys. Chem. B **117**, 11 397 (2013).
[28] L. Onsager, Phys. Rev. **37**, 405 (1931).
[29] L. Onsager, Phys. Rev. **38**, 2265 (1931).
[30] L. Joly, C. Ybert, E. Trizac, and L. Bocquet, J. Chem. Phys. **125**, 204716 (2006).
[31] Q. Ehlinger, L. Joly, and O. Pierre-Louis, Phys. Rev. Lett. **110**, 104504 (2013).
[32] A. E. Ismail, G. S. Grest, and M. J. Stevens, J. Chem. Phys. **125**, 014702 (2006).
[33] Disentangling the two contributions would require a dedicated study and using the sophisticated methods developed recently to identify the intrinsic surface; see, for instance, Ref. [34].
[34] F. Bresme, E. Chacón, and P. Tarazona, Phys. Chem. Chem. Phys. **10**, 4704 (2008).
[35] D. M. Huang, C. Cottin-Bizonne, C. Ybert, and L. Bocquet, Phys. Rev. Lett. **98**, 177801 (2007).
[36] D. M. Huang, C. Cottin-Bizonne, C. Ybert, and L. Bocquet, Langmuir **24**, 1442 (2008).
[37] D. Jing and B. Bhushan, Langmuir **29**, 6953 (2013).
[38] S. Chakraborty, D. Chatterjee, and C. Bakli, Phys. Rev. Lett. **110**, 184503 (2013).
[39] K. G. Marinova, R. G. Alargova, N. D. Denkov, O. D. Velev, D. N. Petsev, I. B. Ivanov, and R. P. Borwankar, Langmuir **12**, 2045 (1996).